JOURNAL OF GEOPHYSICAL RESEARCH, VOL. 113, A09220, doi:10.1029/2008JA013061, 2008

On the relationship between thin Birkeland current arcs and reversed flow channels in the winter cusp/cleft ionosphere

J. Moen,[1,2] Y. Rinne,[1] H. C. Carlson,[1,3] K. Oksavik,[4] R. Fujii,[5] and H. Opgenoorth[2]

Received 25 January 2008; revised 14 March 2008; accepted 1 May 2008; published 16 September 2008.

[1] In this paper we study reversed flow events (RFEs) that seem regulated by Birkeland current arcs in the winter cusp ionosphere above Svalbard. An RFE is a longitudinally elongated, 100–200 km wide channel, in which the flow direction is opposite to the background convection, persisting for 10–20 min. The RFE onset occurs with the brightening of a discrete arc near the open-closed boundary. The auroral arc is situated exactly at a sharp clockwise flow reversal, consistent with a converging electric field and an upward field-aligned current. One category of RFEs propagates into the polar cap in tandem with poleward moving auroral forms, while another category of RFEs moves with the cusp/cleft boundary. The RFE phenomenon is addressed to a region void of electron precipitation, and in lack of direct sunlight the E-region conductivity will be very low. We propose two possible explanations: (1) the RFE channel may be a region where two MI current loops, forced by independent voltage generators, couple through a poorly conducting ionosphere and (2) the reversed flow channel may be the ionospheric footprint of an inverted V-type coupling region. Electron beams of <1 keV will not give rise to significant conductivity gradients, and the form of a discontinuity in the magnetospheric electric field will be conserved when mapped down to the ionosphere, although reduced in amplitude. These two explanations may be related in the sense that the boundary discontinuity in the magnetospheric electric field in (1) may be the driver for the inverted V in (2).

Citation: Moen, J., Y. Rinne, H. C. Carlson, K. Oksavik, R. Fujii, and H. Opgenoorth (2008), On the relationship between thin Birkeland current arcs and reversed flow channels in the winter cusp/cleft ionosphere, *J. Geophys. Res.*, *113*, A09220, doi:10.1029/2008JA013061.

1. Introduction

[2] Since *Haerendel et al.* [1978] and *Russell and Elphic* [1979] discovered transient and spatially limited Flux Transfer Events (FTEs) at the magnetopause, there has been an ongoing search for FTE footprints in the ionosphere. *Goertz et al.* [1985] were the first to relate ionospheric flow bursts observed by the STARE radar to magnetopause reconnection. *Southwood* [1987] put forward a model for FTEs. According to the Southwood model, newly reconnected fast moving flux will set up a local twin vortex flow disturbance. Consistent with this flow picture there will be an upward field-aligned current (FAC) sheet at the clockwise flow shear and a downward FAC sheet at the counter clockwise cell of the flow disturbance, and these are closed via an ionospheric Pedersen current. *Lockwood et al.* [1989] discovered a correspondence between cusp auroral transients and flow enhancements, and this was interpreted by *Sandholt et al.* [1990] as Southwood FTEs. Afterwards there has been a systematic search for three observable elements of the Southwood twin cell model: (1) the newly open fast moving center flux, (2) the upward/dawnward pair of FACs on the flanks of newly open flux, and (3) the proposed return flows on either side.

[3] (1) *Pinnock et al.* [1993, 1995] identified a class of longitudinally extended Flow Channel Events (FCEs) by the PACE HF radar, consistent with the magnetic tension pull on newly open flux. The same category of events was further elaborated and termed pulsed ionospheric flows (PIFs) by *Provan et al.* [1998] and *Provan and Yoeman* [1999]. *Sandholt et al.* [2004] investigated spatial and temporal structures in the dayside aurora and flow channels for southeast IMF orientation. They identified three types of flow channels: (i) on sunward return flow on closed field lines, (ii) on newly open flux containing FTEs, and (iii) on old open field lines. Category (i) was found by *Lockwood et al.* [1993] and *Moen et al.* [1995, 2006] consistent with the *Cowley and Lockwood* [1992] model of flow generation by pulsed reconnection. Category (ii) contains the above mentioned FCEs and PIFs. Category (iii) flow channels were attributed by *Sandholt et al.* [2004], *Farrugia et al.* [2004], and *Sandholt and Farrugia* [2007]

[1]Department of Physics, University of Oslo, Oslo, Norway.
[2]European Space Agency, ESTEC, Noordwijk, Netherlands.
[3]Air Force Research Laboratory, EOARD, London, UK.
[4]Arctic Geophysics, The University Centre in Svalbard, Svalbard, Norway.
[5]Solar-Terrestrial Environmental Laboratory, Nagoya University, Nagoya, Japan.

0148-0227/08/2008JA013061$09.00

to the solar wind magnetosphere dynamo in the high-latitude boundary layer [*Stern*, 1984]. It should be noted that flow directions for all these categories are consistent with the large scale polar cap flow pattern. In this paper we will examine a fourth category of flow channels, the reversed flow events (RFEs) defined by *Rinne et al.* [2007]; reversed by means of flow opposing the background convection. We will come back to a more detailed description.

[4] (2) Candidate signatures of the FAC system of the Southwood FTE model have been reported in a series of papers. Sandholt and coworkers proposed that poleward moving auroral forms (PMAFs) are the optical footprint of the upward FTE current sheet [e.g., *Sandholt et al.*, 1990; *Sandholt and Farrugia*, 2007, and references therein]. Similarly, *Milan et al.* [2000], *McWilliams et al.* [2001], and *Lockwood et al.* [2001] located east–west elongated arcs observed by Polar UVI on one side of cusp flow channels consistent with an FTE current system. By direct measurements of FACs *Marchaudon et al.* [2004] placed a pair of upward and downward sheet currents on each side of a flow channel observed by SuperDARN consistent with the Southwood FTE model.

[5] (3) The final test of the Southwoood FTE model was to observe return flow channels. *Lockwood et al.* [1990] proposed that the return flow around Southwood FTEs may not be pronounced, but rather give rise to a reduction in the background flow. *Pinnock et al.* [1993] noticed a reduction in the background flow. *Thorolfsson et al.* [2000] carried out a detailed study of distorted flow around poleward moving auroral forms (PMAFs) combined with SuperDARN and optical data. They found clear evidence for return flow near the eastward and westward edges of east–west elongated PMAFs, consistent with their own simulation of Southwood FTEs, but no continuous return flow channels were to be expected.

[6] The Special Norwegian Fast Azimuth Scan Mode (SP-NO-FASM) on the EISCAT Svalbard Radar (ESR) provides a new important tool to map mesoscale flow structures in much greater detail. Applying this technique, *Oksavik et al.* [2004, 2005] were the first to observationally map out a clockwise flow shear around an east–west elongated PMAF that is consistent with an upward FAC sheet. They reported evidence for a twin-cell signature in support of the Southwood FTE model. *Rinne et al.* [2007] introduced the new term, reversed flow events, to characterize ~100–200 km wide east–west elongated channels that exceed the ESR field of view (~600 km) and have an average life time of ~18 minutes, i.e., quasi-static flow structures. In a systematic search through the SP-NO-FASM database of winter cusp observations, *Rinne et al.* [2007] did not find RFEs that developed in pairs, as the twin-cell FTE model predicts. Because the RFEs always occurred as east–west elongated channels, *Rinne et al.* [2007] proposed an asymmetric version of the Southwood FTE model, in which return flow develops predominantly on the poleward side of newly open flux since on the equatorward side it is inhibited by the open-closed boundary (OCB) boundary.

[7] The aim of this paper is to reveal more information about RFE flow channels and examine their relationship to discrete arcs/Birkeland currents sheets. Each RFE develops with the intensification of a discrete arc, consistent with converging electric fields and a sheet of upward FAC. The RFE phenomenon contains PMAFs as reported by *Oksavik et al.* [2004, 2005] but is not exclusively related to this category. They rather appear to be a specific feature of a Birkeland current arc system and we will propose two new explanations for the RFE phenomenon. In one explanation the RFE electric field, E_{RFE}, develops in the gap between two MI current loops. The other explanation links the flow perturbation to an auroral acceleration region.

[8] The paper is organized as follows. The instrumentation is briefly described in the following section. Section 3 presents combined radar and all-sky observations of RFEs observed on 16 and 20 December 2001. The observations are discussed in section 4, and section 5 provides a summary and concluding remarks.

2. Instrumentation

[9] The EISCAT data used in this study were obtained by the Special Norwegian Fast Azimuth Scan Mode (SP-NO-FASM [*Carlson et al.*, 2002]) that utilizes the 32 m steerable antenna at Longyearbyen (78.15°N, 16.03°E). The antenna beam was moved as a windshield wiper over the azimuth range from 180° to 300° at the lowest possible elevation of 30^0. The azimuth angle increases clockwise from geographic north. Geomagnetic north corresponds to 328° azimuth. At a slew speed of 0.625°/s it takes 192 seconds to complete one scan in each direction. During a scan data is stored every 3.2 s giving 60 adjacent beams each 2 degree wide in azimuth. The radial resolution is about 40 km and the azimuth resolution is varying from 10 km to 30 km with increasing distance from the radar. The altitude of the radar gates is increasing from 116 km at range 226 km to 585 km at range 1050 km.

[10] The all-sky imager located at Ny-Ålesund (78.92°N, 11.95°E) acquired 6 images per minute, one 630.0 nm image every 30 second followed by two 557.7 nm images. The exposure time was 1 sec for the 630.0 nm wavelength and 0.5 sec for the 557.7 nm wavelength. The aurora was red-dominated and we are only going to present 630.0 nm images projected on a geographic frame of reference assuming 250 km as the peak emission altitude.

[11] The Interplanetary magnetic field (IMF) and plasma parameters of the solar wind were obtained from the ACE spacecraft [*Chiu et al.*, 1998] located near the L1 point. In this paper we will present data from the magnetic field experiment [*Smith et al.*, 1998] and the Solar Wind Electron Proton Alpha Monitor (SWEPAM [*McComas et al.*, 1998]).

[12] SuperDARN convection maps [*Ruohoniemi and Baker*, 1998] are used to frame the large scale flow context of the mesoscale flow channels observed by ESR. These convection maps have been reanalyzed to yield IMF conditions for the estimated time lag.

3. Observations

3.1. 16 December 2001

[13] Figure 1a illustrates the fan swept by ESR in the framework of the SuperDARN convection map for 10:30–10:32 UT on 16 December 2001. The radar field of view spanned from ~12:00–13:30 MLT. The cusp inflow region was shifted several hours prenoon due to a strong IMF B_Y positive, and the ESR scan region was situated under north-

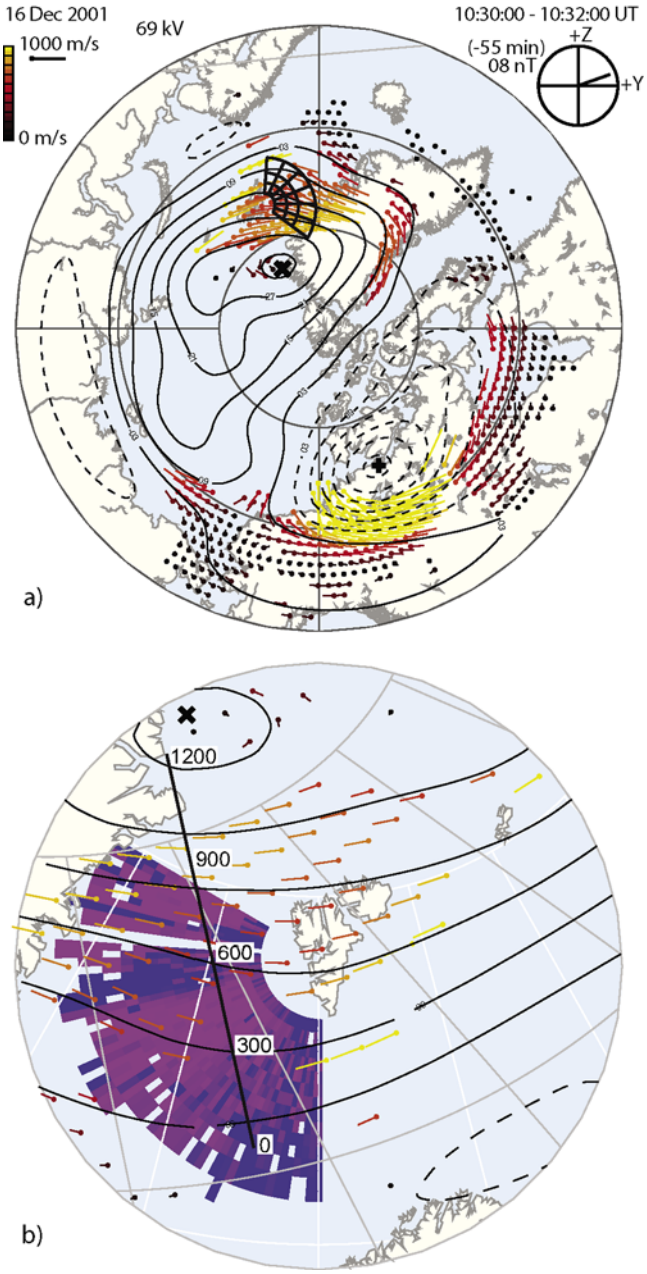

Figure 1. (a) SuperDARN convection map obtained for 10:30 UT on 16 December 2001. The fan-shaped grid located between Svalbard and Greenland indicates the ESR field of view. (b) Comparison of SuperDARN convection vectors and high-resolution velocity data measured by ESR west of Spitsbergen. Pink color in the ESR fan means line-of-sight velocity away from the radar, and blue color means flow toward the radar. The narrow blue channel elongated east–west between Svalbard and Greenland represents a reversed flow event, opposing the large scale background convection. The black measure bar from 0 to 1200 km indicates the orientation of the line used to stripe out keograms from all-sky data in Figures 4h and 5h.

westward flow of the afternoon cell. Figure 1b presents the line-of-sight velocity observed during the clockwise ESR scan from 10:29.04–10:32.12 UT together with SuperDARN convection vectors from Figure 1a. Pink color means away flow and blue means toward flow. The reversed flow event (RFE) is the blue channel elongated east–west between Svalbard and Greenland. The pink away flow is consistent with the north-westerly oriented large scale convection. However, it is the blue RFE channel of flow opposing the background that is of particular interest for this study. The black measure bar (0–1200 km) west of Spitsbergen marks the line from where we are going to present all-sky keograms (Figure 4h and Figure 5h). The ~100 km wide RFE channel was not resolved by the SuperDARN radars, probably due to a nonideal geometry.

[14] ESR scanned the area between Greenland and Svalbard from 09:30 UT to 11:00 UT. Rows 1–6 in Figure 2 display line-of-sight velocity data for six consecutive scans from 10:13–10:32 UT. Start and stop times (UT) for each ESR scan and the scan direction, clockwise (cw) or counter clockwise (ccw), are given on the top of each radar plot. Column 1 displays only the positive line-of-sight velocities radially away from the radar (negative values have been whitened out). This is complemented by column 2 that displays only the negative line-of-sight velocities (positive values have been whitened out). The first scan (10:13.04–10:16.12 UT) is entirely consistent with the large scale convection monitored by SuperDARN. Nearly homogenous strong westward flow (~1 km s^{-1}) is directed away from the radar (red color) in Sectors 4–6. Then there is a sharp transition to a blue region of weak flow further south. Comparing the first and the second row, the onset of a flow disturbance (Fs) occurred in the equator-most region of strong away flow, indicated by an arrow in Frame (2,1). In row 3 (10:19.28–10:22.36 UT) the reduced flow signature had developed in length to ~400 km, and the velocity at the centre was close to zero. In the subsequent scan ~3 minutes later (10:22.40–10:25.48 UT) the flow structure had developed in strength and size to accomplish the RFE definition introduced by *Rinne et al.* [2007]: the line-of-sight velocity inside the RFE must be larger than 250 m s^{-1} in at least 1 scan and a longitudinal extent of at least 400–600 km. The event presented in Figure 2 is RFE #10 in the statistical work by *Rinne et al.* [2007]. In the subsequent scan RFE10 exceeded the longitudinal extent of the ESR field of view (>600 km) and was ~150 km wide (Frame (4,1)). As annotated on the top row in Figure 2, the ESR field of view is subdivided in 6 wedge formed Sectors, 1 to 6 increasing clockwise, and 3 regions a–c with increasing distance in range. There are 10 beams in each sector. In order to quantify the flow disturbance of RFE10, we introduced a low-pass noise filter by averaging the velocity numbers for ~5 radar gates selected along iso-contours of the flow channel in Region b, Sectors 3–6. In the third column the averaged velocity numbers have been plotted referring to the ESR Beam number 21–60 from Sectors 3–6. From Frame (4,3) we see a flow minimum of −400 m s^{-1} within the RFE. RFE10 was located at nearly the same position in Row 5 (10:25.52–10:29.00 UT), the reversed flow had slightly reduced and the width had narrowed to ~100 km. It is also noticed that the flow equatorward of the channel had increased. 3 minutes later in Row 6, the equatorward boundary of RFE 10 had moved 100 km north, corresponding to an average drift speed of ~0.5 km s^{-1}. The westward flow equatorward of the RFE

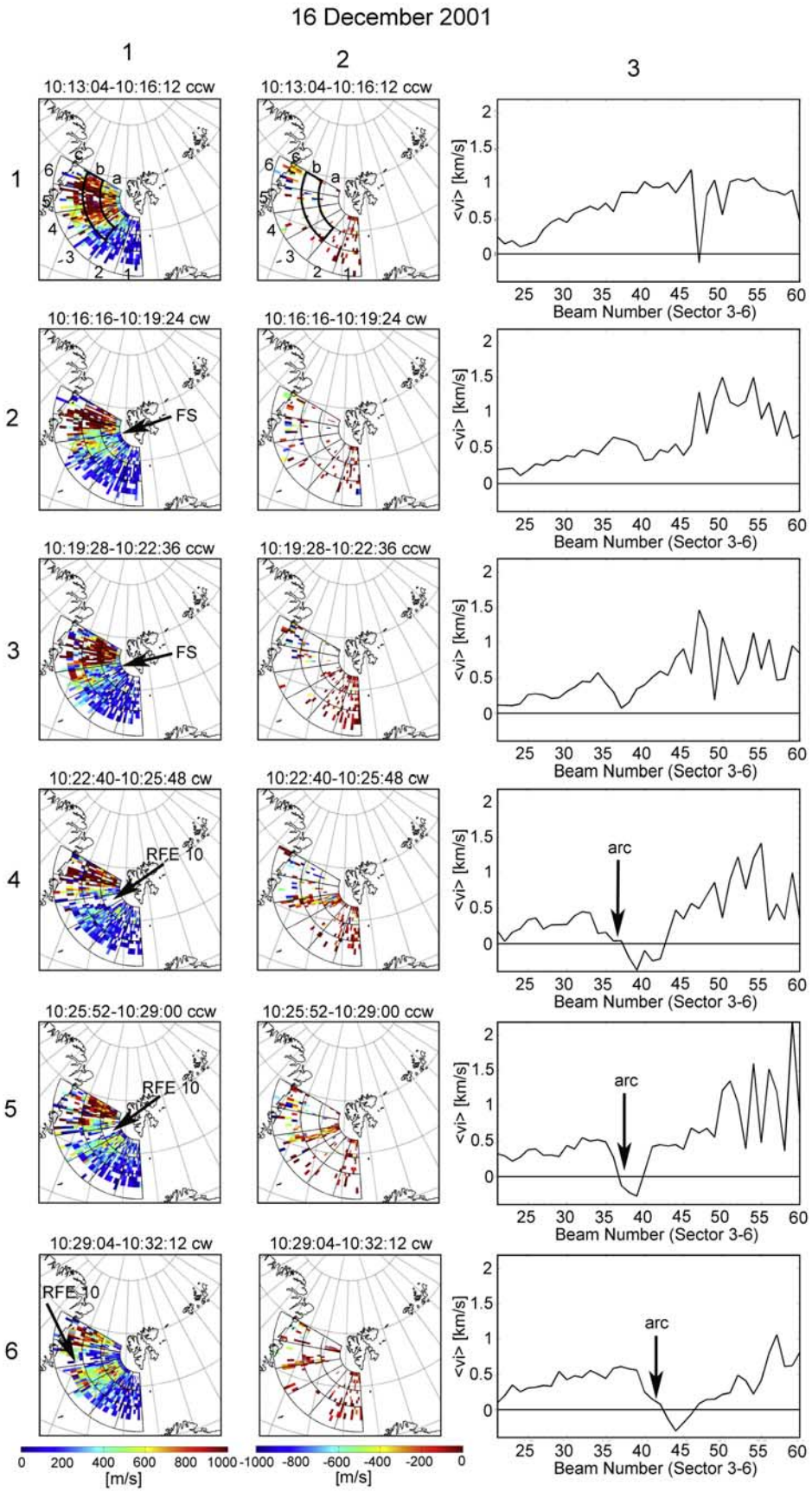
16 December 2001
1
2
3
10:13:04-10:16:12 ccw
10:16:16-10:19:24 cw
10:19:28-10:22:36 ccw
10:22:40-10:25:48 cw
10:25:52-10:29:00 ccw
10:29:04-10:32:12 cw
FS
RFE 10
arc
<vi> [km/s]
Beam Number (Sector 3-6)
0 200 400 600 800 1000
-1000 -800 -600 -400 -200 0
[m/s]

Figure 2

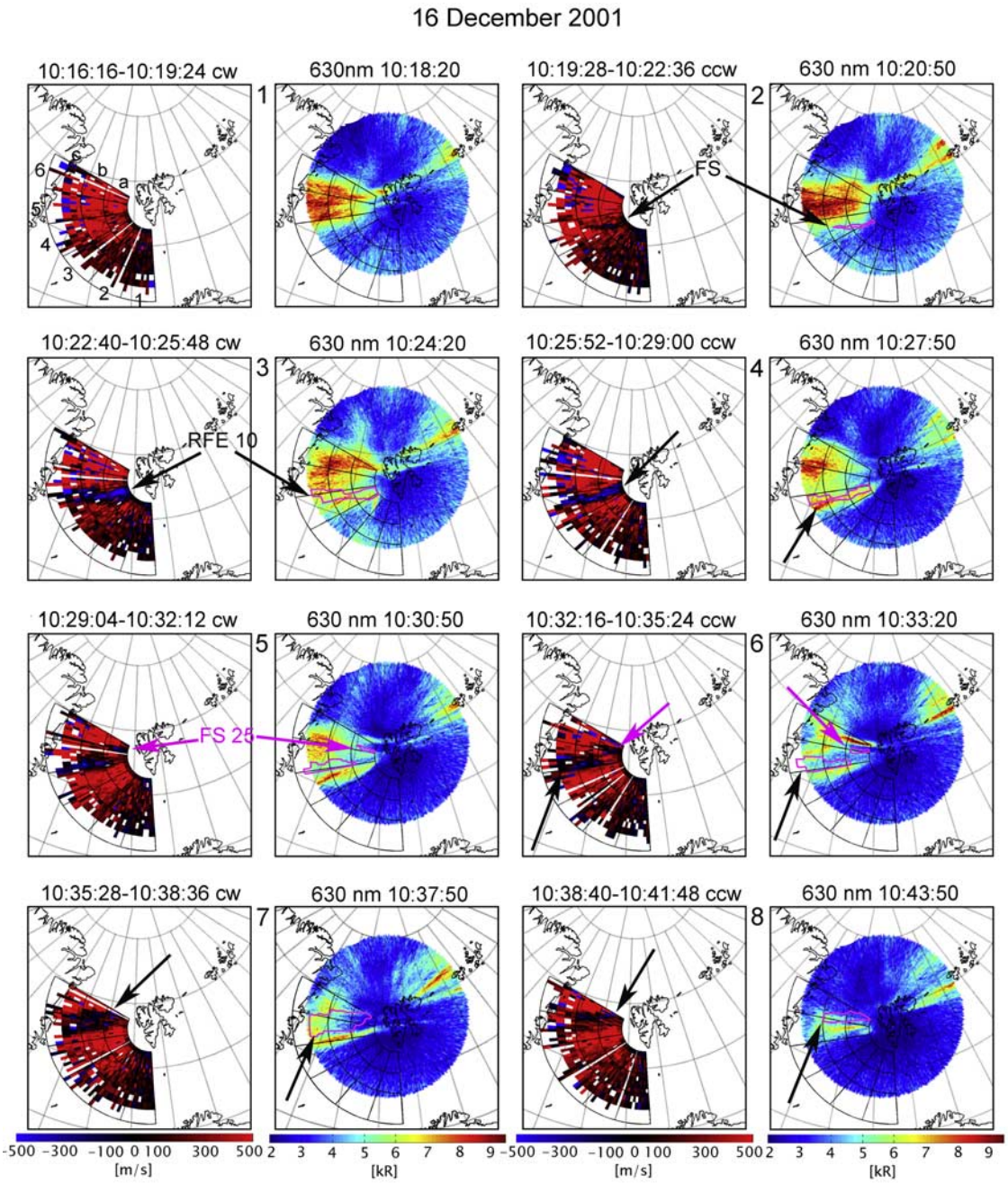

Figure 3. ESR velocity data side by side with 630.0 nm all-sky data. The ESR and the all-sky data have both been projected to 250-km altitude. The Fs (flow signature) and RFE10, indicated by arrows in the ESR scans, are ringed out with pink contours on the corresponding all-sky data. Please note that RFE10 is located on the poleward side of a discrete auroral form.

had increased further. The RFE had almost disappeared from Sector 5a, indicating it had moved westward, or, a gradual fade had started from the eastern end.

[15] In Figure 3, the evolution of RFE10 is placed in the context of the auroral morphology. A selection of 8 radar scans acquired during a half hour interval from 10:16.16–10:43.50 UT is presented side by side with the corresponding 630.0 nm all-sky image. As the 630.0 nm all-sky image was updated 6 times during each radar sweep, we have presented all-sky images from the middle of each

Figure 2. Column 1 displays positive line-of-sight velocities measured by ESR for six consecutive azimuth scans from 10:13 to 10:32 UT. Column 2 displays the corresponding negative line-of-sight velocities. Column 3 presents averaged velocity along RFE 10 in Region b, Sectors 3–6. This part of the ESR sweep is marked out with a black contour in Frame (1,1) and (1,2).

scan. The all-sky camera log book reports thick clouds around 08:00 UT, a slight weather improvement around 09:20 UT. At 10:15 UT it was reported clear sky with some clouds at the southern horizon, and entirely clear sky from 10:45 UT. In the image sequence, the cloud contamination is seen as turquoise glow in the southern part of the field of view that gradually faded. The aurora was dominated by the 630.0 nm line, and the 630.0 nm all-sky images have been projected to a common reference altitude of 250 km. The ESR reference grid has been overlaid on the all-sky images to ease the comparison. The all-sky data have been adjusted for zenith angle effects (loss of sensitivity toward the horizon), calibrated and plotted in kR with a color scale ranging from blue to red with increasing intensity. As pointed out by *Moen et al.* [1995] one has to execute care when dealing with projected data. Long auroral structures pointing at the observation site indicate the presence of tall rays projected to one altitude. The upper part of a tall ray filament will appear at a shorter radial distance from the observation site than the lower altitude part. For an auroral form that is located south of the observation site the part that is farthest away (i.e., at highest zenith angle) represents the bottom end of tall rays.

[16] Svalbard was situated near the transition between two different regimes of auroral activity. East of Svalbard in the direction of Franz Josef Land, the activity was less intense and we see examples of multiple arcs, which could be of boundary plasma sheet origin [*Sandholt et al.*, 1998]. In contrast, the cusp type auroras west of Svalbard were much more intense, a broad region with strong intensifications in the 630.0 nm aurora. A movie of the image sequence revealed episodes of eastward expansions of this cusp aurora followed by westward retreats. The first three images in Figure 3 (10:18.20–10:24.20 UT) demonstrate the end of such an eastward expansion, followed by a westward retreat out of the all-sky field of view (10:27.50–10:43.50 UT). The equatorward expansion arises through the appearance of a new auroral form equatorward of the preexisting activity at 10:24.20 UT. This new auroral form represents the new activity boundary that subsequently retreats poleward. In frame pair 3, the pink contour located adjacent to the new auroral form on the poleward side, represents the contour of RFE10 observed by ESR. In the following sequence, the auroral form and RFE10 moved together; that is, the auroral form stayed fixed to the equatorward border of RFE10 during the rest of its lifetime. Notably, the auroral form is situated near the clockwise flow reversal. A flow signature, Fs25, is annotated in ESR scans 5 and 6. It is sandwiched between two auroral brightenings. In frame pair 7 (10:37.50 UT) these two auroral filaments and Fs25 had disappeared.

[17] Figures 4a–4e presents solar wind plasma and IMF conditions for the period of interest, Figure 4g presents time variations in the SuperDARN polar cap potential, and Figure 4h presents a 630.0 keogram derived from the all-sky imager along the black line drawn across the ESR field of view in Figure 1b. The ACE satellite was located around $[X, Y, Z]_{GSM} = [239, 29, 2]R_E$. The radial solar wind velocity was around 530 km s^{-1} which means an advection time of ~50 minutes from ACE to the magnetopause. Since ACE was off the sun–earth axis by 29 R_E we used the formula provided by *Lockwood et al.* [1989] and found the time lag to be varying between 50–60 minutes, and we introduced a time shift of −55 min for the ACE data. IMF B_Y was steadily positive (~10 nT) throughout the one hour time interval presented. IMF B_Z fluctuated but was predominantly positive. A brief negative excursion occurred at the end of the primary time interval but it is not considered to have any relationship to RFE10. However, it may be related to a narrowing of the auroral activity. IMF B_X underwent large fluctuations as well, but was predominantly negative.

[18] In Figure 4h, the poleward and the equatorward flow reversal boundaries of RFE 10 are drawn as the two pink lines for the duration of the event from 10:22 UT to 10:39 UT. It is clear that the onset of the RFE occurred in association with the brightening of a new discrete auroral form equatorward of the previous activity. The discrete auroral form stayed close to the equatorward edge of RFE 10 during the 17 minute lifetime of the event. The auroral form and the boundary moved poleward together. The location of the auroral form at the flow reversal is confirmed by ESR. It gave rise to discrete intensifications in the electron concentration below 200 km consistent with particle impact ionization exactly at the equatorward edge of the RFE (data not presented). A subsequent reversed flow event, RFE11, was detected by ESR at 10:56 UT, and was seen in only two scans before the radar experiment was stopped. From Figure 4h the onset of RFE11 was also associated with the occurrence of an auroral form equatorward of the previous activity.

[19] The broad cusp activity poleward of the RFE covered Sectors 5 and 6 of the radar fan, was associated with strong north-westward flow seen by SuperDARN. Figure 4g presents the SuperDARN Polar Cap Potential. The cross polar voltage was pulsed between 60–80 kV with 4 maxima in one hour. There is no apparent relationship between the pulsing in the local cusp luminosity and the global polar cap potential. The onset of RFE10 occurred 5 minutes prior to the onset of the enhanced polar cap potential. The duration of RFE10 and the enhanced polar cap potential was about the same. The polar cap potential was decaying during the onset of RFE11.

3.2. 20 December 2001

[20] Figure 5 presents observations from 20 December 2001 in the same format as Figure 4. The ACE data has been time shifted 70 minutes to account for the approximate signal delay between ACE and the ionospheric response. IMF Bz was steadily negative around −5 nT until 10:50 UT when it rapidly turned to +5 nT and then back negative 7 minutes later. The ESR scanned the same area as on 16 December, and monitored northwestward flow of the afternoon cell. It continuously swept this area from 10:06 UT to 10:58 UT. The auroral activity displayed in Figure 5h represents the classical sequence of PMAFs. The onset of RFE18 occurred in the middle of a sequence of poleward moving forms (PMAFs). The RFE developed in association with a new auroral form, on the poleward side. This RFE event moved poleward in tandem with the PMAF. By definition of reversed flow, the RFE faded around 10:42 UT, but a reduction in the background flow

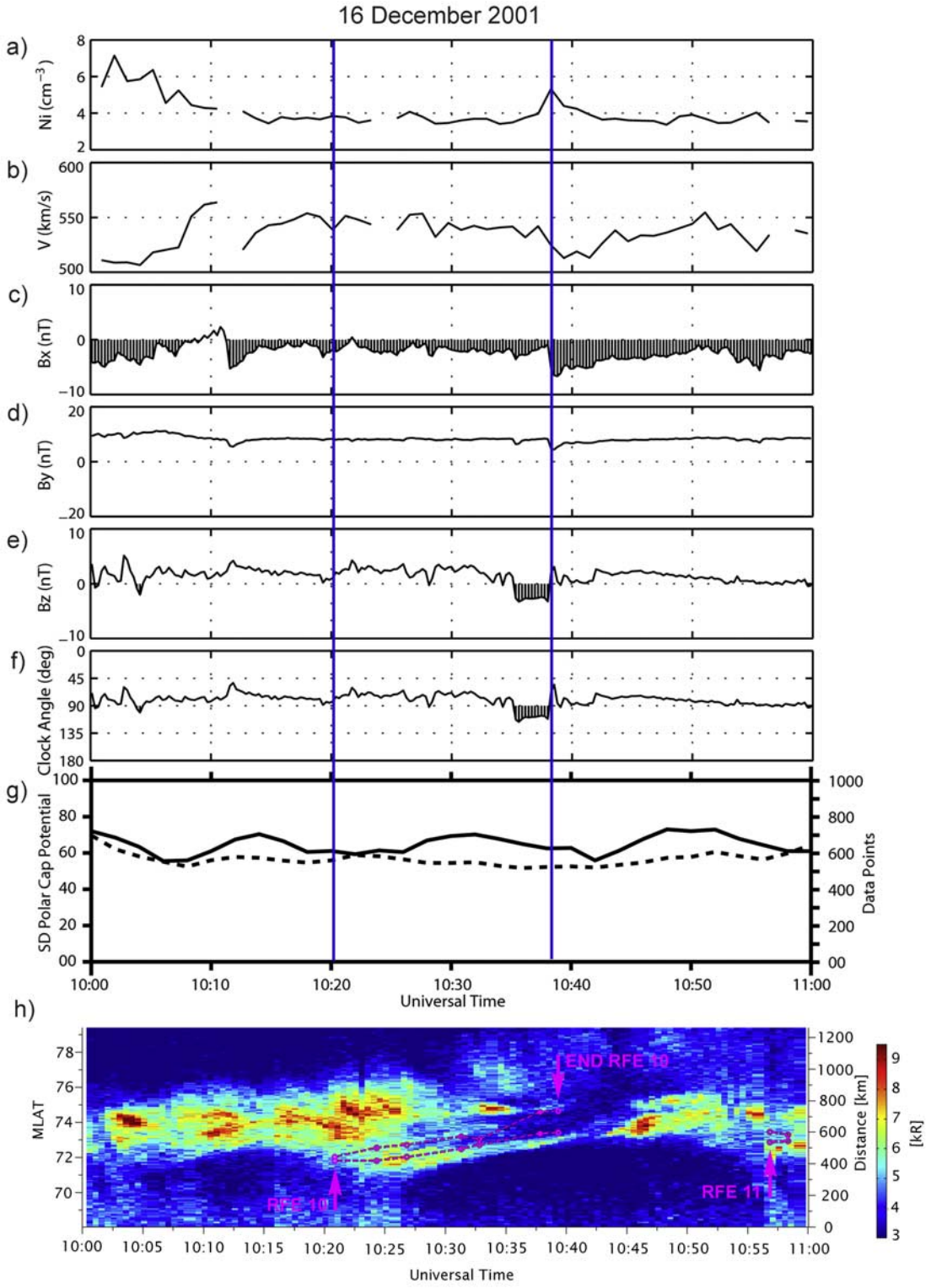

Figure 4. (a–f) Solar wind parameters from the ACE satellite measured in GSM coordinates on 16 December 2001 and shifted in time to correspond with ground observations from 10 to 11 UT. The IMF clock angle increases from 0° due north to 180° due south. (g) The solid curve represents the northern hemisphere polar cap potential (kV, left axis) derived from SuperDARN convection maps. The dashed curve represents the number of data points (right axis) from which the convection maps were calculated. (h) Color-coded 630.0 nm emission intensity (kR) versus time and MLAT along the black measure bar in Figure 1b (also given on the right axis). The pink lines mark the RFE boundaries. The vertical blue guidelines in panels a–g mark the duration of RFE10.

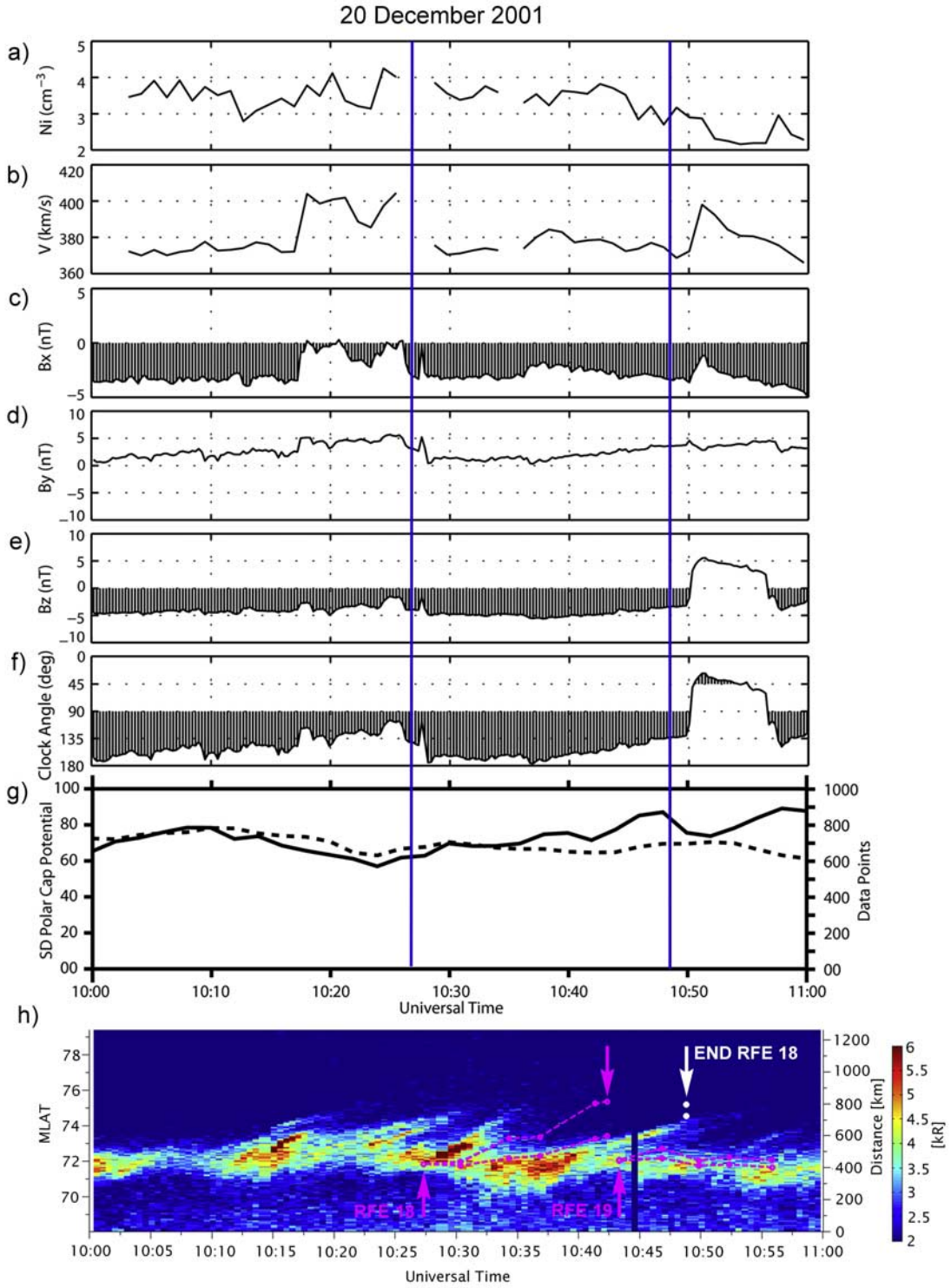

Figure 5. Solar wind, SuperDARN, and optical data for 10 to 11 UT on 20 December 2001, presented in the same format as Figure 4. The vertical blue guidelines in panels a–g mark the duration of RFE18.

was observed until 10:48 UT, marked by the two white dots, that is, as long as the PMAF was observed. The subsequent event (RFE19) also occurred in association with a brightening auroral form. However, instead of moving poleward with the faint PMAF that broke loose from the background arc around 10:53 UT, it stayed with the bright background arc. Traces of particle impact ionization were observed at the equatorward edge of both RFE 18 and 19; that is, the discrete auroral forms were located on the clockwise flow reversal.

[21] Although the RFE onsets occurred in association with increased polar cap potential, over their life time there is no clear trend between RFEs and the modulation of the polar cap potential. The RFE-FAC system is likely to be part of a localized current–voltage system.

4. Discussion

4.1. Observation Summary

[22] Up to now we only have three days of combined radar and optical observations of reversed flow events (RFEs). One of these days was reported by *Oksavik et al.* [2004, 2005] and the other two days were presented in section 3 above. *Oksavik et al.* [2005] analyzed a sequence of RFE channels located on the poleward side of discrete PMAFs, in the sense consistent with a clockwise flow shear and an upward FAC. Their RFEs occurred under conditions of IMF B_Y positive and IMF B_Z negative. With regard to the auroral morphology, the situation is more complex on 16 December 2001 presented here when IMF B_Z and B_Y are both positive (Figure 4). RFE 10 occurred in association with a brightening arc filament equatorward of a broad region of preexisting cusp type auroral activity. Also, in this case, the RFE clockwise flow shear is collocated with a discrete auroral form consistent with an upward Birkeland current sheet. The RFE and the Birkeland current arc moved poleward in tandem, and the RFE disappeared when the arc fainted. On 20 December 2001, IMF B_Z was south and IMF B_Y was positive, and the classical sequence of PMAFs was observed (Figure 5h). On this day, RFE18 moved in tandem with a PMAF, but RFE19 did not; it stayed with the background instead of breaking loose to follow a weak PMAF. It should however be noted that no RFE occurrence does not necessarily mean lack of flow disturbance. *Rinne et al.* [2007] reported a flow structure (Fs30) lasting from 10:16–10:25 UT, and from Figure 4h we see that a weak but discrete PMAF actually separated from the background aurora during that time interval. Fs25 in Figure 3 occurred between two arc filaments (frame 5 and 6). Hence the RFEs may represent the ''top of the iceberg'' of flow disturbances, strong enough to reverse the flow, while the less prominent flow structures may be related to a flow reduction only.

[23] Most of the RFEs documented so far developed post noon, near the equatorward boundary of the cusp inflow region for IMF B_Y positive. However, the current SP-NO-FASM database is strongly biased toward IMF B_Y positive [*Rinne et al.*, 2007].

[24] In contrast, to the three categories of flow channels reported by *Sandholt et al.* [2004], all speeding up the large scale convection pattern, the RFE category reverts the background flow (cf. Introduction). The RFEs reported here occurred in the afternoon cell, as 100–200 km wide channels of eastward flow, i.e., flow opposing the magnetic tension pull for IMF B_Y positive. *Farrugia et al.* [2004] reported antisunward (eastward) flow bursts in the same time sector, but for IMF B_Z negative. Their flow events occurred in a broad region of antisunward flow, poleward of a well-defined flow reversal consistent with a crescent shaped dusk cell. Their flow bursts were in same direction as the background flow and attributed to the solar wind magnetosphere dynamo in the high-latitude boundary layer [*Stern*, 1984], i.e., fundamentally different from RFEs.

4.2. Comments on the FTE Twin-Cell Explanation for RFEs

[25] The connection between PMAFs and RFEs was readily documented by *Oksavik et al.* [2004, 2005]. In a statistical work *Rinne et al.* [2007] found that all their flow events (31 flow structures and 21 RFEs) were scattered within the IMF clock angle range from 40–240°, i.e., within the wide range of clock angles (30–330°) for which bursty reconnection at the magnetopause may occur [*Neudegg et al.*, 2000]. *Oksavik et al.* [2004, 2005] interpreted the reversed flow channels in terms of the return flows of the twin-cell FTE model by *Southwood* [1987]. However, there are problems with this FTE explanation:

[26] (1) *Rinne et al.* [2007] did not find evidence for RFEs developing in pairs as the twin-cell FTE model predicts. In cases when two RFEs coexisted within the radar field of view there was ~10–30 minutes delay in the onset time between the first and the second event.

[27] (2) The RFE channels remain extremely narrow during their life time. The RFE channels are usually around 100 km wide but up to 250 km on occasion. In the rest frame of a Southwood FTE event there will be return flow on either side of the newly opened centre flux moving fast under the action of the magnetic tension force, pushing its way through the ambient plasma moving more slowly. In the case of no background flow, one would also see the return flow in the rest frame of the radar. Due to incompressibility the return flow pattern will broaden very quickly. However, in the normal case when one event after the other superimposes on decent background convection, the ''return'' flow around each event should rather appear as reductions in the background flow, as suggested by *Lockwood et al.* [1990] and *Pinnock et al.* [1993], and simulated by *Thorolfsson et al.* [2000].

[28] (3) The category of PMAF events in the cusp have been attributed to transient magnetopause reconnection [e.g., *Sandholt et al.*, 1990, 1993; *Denig et al.*, 1993; *Milan et al.*, 1999, 2000; *Thorolfsson et al.*, 2000; *Moen et al.*, 2001]. From Figure 5 we noted that the RFE phenomenon does not uniquely relate to the category of PMAFs; RFE 19 stayed with the background arc.

[29] Let us now consider an FTE approach on RFE10 on 16 December (Figures 2, 3, and 4). RFE10 and the associated Birkeland current arc developed equatorward of a broad region of cusp precipitation (cf. Figure 3 and Figure 4h). From the image sequence in Figure 3 the broad region of intense cusp auroral activity at the beginning subsequently faded and/or moved westward out of the all-sky field of view. RFE10 moved with the trailing edge of the cusp activity. Assume that the arc brightening was part of an FTE event. In this case when IMF B_Y was large and positive, the initial magnetic tension on newly open flux is expected to have a strong westward component [*Cowley et al.*, 1991]. This excludes the RFE channel itself from being the newly opened flux, but potentially it could represent the return flow on the poleward side of the newly opened flux region [*Oksavik et al.*, 2004, 2005; *Rinne et al.*, 2007]. For IMF B_Y large positive, a longitudinally elongated channel of newly opened flux pulled westward, will be bounded by an upward FAC sheet on the poleward edge and a downward FAC sheet on the equatorward edge [*Taguchi et al.*, 1993]. However, if the Birkeland current arc actually

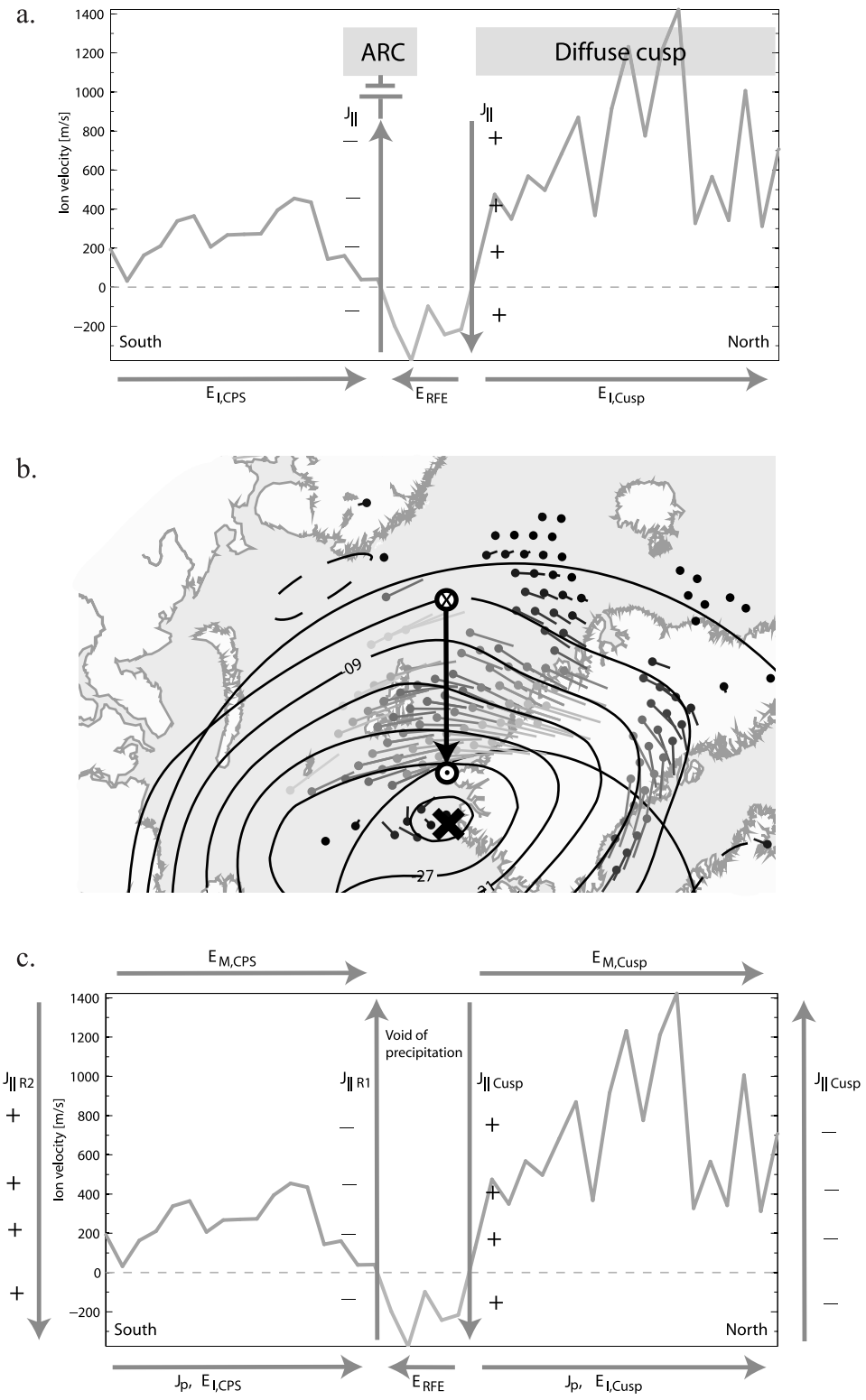

Figure 6. (a) A schematics to summarize the observations of RFE10 on 16 December 2001. The ⟨vi⟩ curve is from Figure 2. ⟨vi⟩ negative east corresponds to a southward electric field within the RFE flow channel. ⟨vi⟩ positive west corresponds to a northward electric field addressed to the closed magnetosphere equatorward of this channel, and open cusp field lines correspond to poleward of this channel. The discrete arc represents an upward FAC at the clockwise flow reversal boundary. (b) The large scale north electric field vector associated with the dusk cell overlaid the SuperDARN flow pattern as shown in Figure 1 for 10:30 UT on 16 December 2001. (c) A schematic illustration of the RFE phenomenon that occurs between two current loops, forced by two separate voltage generators. The E_{RFE} is located in a region void of precipitation.

marked the poleward border of newly opened flux, the region of newly opened flux equatorward of it was invisible to our all-sky imager. Newly opened flux is supposed to be associated with bulk injection of magnetosheath plasma, and magnetosheath electron precipitation efficiently heats F2 region electron plasma [*Lockwood et al.*, 1993; *Waterman et al.*, 1994; *Nilsson et al.*, 1996; *Pryse et al.*, 2000; *Doe et al.*, 2001; *Moen et al.*, 2004b]. With certain constraints the elevated electron temperature (T_e) can be used to identify the cusp open-closed boundary [*Doe et al.*, 2001; *Moen et al.*, 2004b]. ESR did observe elevated T_e with the discrete auroral form, but not equatorward of it. This makes us conclude that the RFE10 Birkeland current arc was either located on closed field lines, or it was a signature of the OCB. That is, we discard the possibility of newly open flux equatorward of the RFE10 channel and the RFE10-Birkeland current arc system does not fit into the FTE picture anticipated.

[30] On December 20 in Figure 5 on the other hand, a broad 630 nm flash, ~2 degrees in latitude, was observed equatorward of RFE18 at the beginning, before it narrowed to a thin arc at ~10:42. This region was associated with elevated T_e observed by ESR (data not presented). The flash region may indeed signalize the expected bulk injection of magnetosheath electrons on newly opened field lines, bounded with an upward FAC sheet on the poleward side and a downward FAC sheet on the equatorward side. That is, RFE18 is consistent with a PMAF-FTE signature for IMF B_Y positive and B_Z negative.

4.3. Relationship Between RFEs and Birkeland Current Arcs

[31] For all the RFEs observed with complementary optics, the clockwise shear does always develop together with a discrete auroral form consistent with an upward Birkeland current sheet. Discrete auroral forms represent a footprint of accelerated electron precipitation. There are two acceleration mechanisms frequently observed above the ionospheric cusp: Kinetic Alfvén waves (KA waves [*Chaston et al.*, 2007]) and inverted Vs [*Lin and Hoffman*, 1982]. Inverted V-type electron precipitation gives rise to monoenergetic beams while dispersive KA waves give rise to a broader energy range within the beam [*Chaston et al.*, 2007]. The maximum energy of KA waves is very similar to that reported for dayside inverted Vs [*Lin and Hoffman*, 1982], both around 1 keV. Inverted Vs and KA waves can easily be distinguished from each other in satellite and rocket data, while more difficult from ground.

[32] The schematics in Figure 6a is based on the averaged $\langle v_{los} \rangle$ curve in Frame (4,3) of Figure 2. Superimposed on this plot is the location of the Birkeland current arc, and the diffuse 630.0 nm auroral cusp region that straddled the northern part of the radar field of view. It is noted from Figure 3.1, that intense cusp auroral activity covered Sectors 5 and 6 of the ESR fan, while the region of strong flows covered Sectors 4–6. That is, the background of strong westward flow was extended well equatorward of the cusp auroral boundary, taken as a proxy of the open-closed boundary [*Moen et al.*, 1996, 1998]. The electric field $E_{I,\ CPS}$, south of the discrete arc structure is located at subauroral latitudes. $E_{I,CUSP}$ is the electric field associated with the strong westward flow in the auroral cusp region. E_{RFE} is situated in a region void of auroral precipitation. The most poleward flow reversal (counter-clockwise) is consistent with a downward current.

[33] Let us now put these observations in the context of expected large scale current systems. Figure 6b illustrates the convection electric field vector consistent with sunward flow in the dusk cell. As indicated this E-field vector requires a downward FAC near the equatorward boundary of the dusk cell and an upward FAC at the dusk cell flow reversal. The poleward part of this vector was straddled with cusp auroral activity on open field lines.

[34] The portion of this vector at subauroral latitudes; that is, equatorward of the discrete auroral form was likely mapping to the central plasma sheet (CPS). On the top of Figure 6c, we have therefore indicated two different electric fields forcing a westward movement of ionospheric plasma; $\mathbf{E}_{M,CUSP}$ and $\mathbf{E}_{M,CPS,}$ representing open and closed flux, respectively. The RFE channel itself could be on open or it could be on closed field lines. Anyway, this idealized picture suggests two different MI-current loops. One is the Region 2–Region 1 current system on closed field lines, and the other is the large scale cusp current system forced by the solar wind. The polarity of the cusp current system is consistent with reconnection for IMF B_Y positive [*Taguchi et al.*, 1993]. In this large scale perspective, the RFE convection channel was located at the boundary between two different current systems mapping to widely different flow generators in the magnetosphere. In this perspective, it appears that the E-field discontinuity associated with RFE10 developed locally at a boundary transition region. According to the auroral arc classification made by *Marklund* [1984], the RFE flow signature bear resemblance to his category II_b of Birkeland current arcs, with a double flow reversal.

[35] We can think about two possible explanations for the RFE phenomenon:

[36] (1) In Figure 6c, the E_{RFE} is located in between two MI-current loops, each forced by a separate voltage generator. For this particular case one loop was on open field lines and the other loop appears to be on closed field lines. However, in a sequence of RFEs/PMAFs as presented by *Oksavik et al.* [2005], it could be that successive current loops map to distinct reconnection sites. The major point here is that each current loop is forced by an independent voltage generator, and that there is a small gap or E-field discontinuity between them. RFE10 was located between the discrete auroral form and the cusp auroral activity, i.e., in a region void of precipitation. In absence of solar EUV ionization in the E and lower F region, this means very low height-integrated Pedersen conductivity there. A large E_{RFE} arises if the two current loops at different potential couple through the low conducting ionosphere. Low Pedersen conductivity and poor cross coupling provides an explanation for the long life time.

[37] (2) The bipolar form of RFE10 may possibly be the ground signature of an inverted V acceleration region. As was noted in Figure 2 the background flow was gradually suppressed in the development phase of RFE10. This may indicate a partial decoupling from the magnetosphere due to a field-aligned potential drop. A dayside inverted V is

typically of the order of 1 keV and it will have a very different effect on the ionosphere than a nighttime inverted V of the order of 10 keV.

[38] Due to the relatively long life time RFEs can be treated as a quasi-stationary phenomenon. Assuming that the E and F region neutral winds are negligible compared to the $E_\perp \times B$ drift, the current density perpendicular to the electric field can be written as

$$j_\perp = \sigma E_\perp + \sigma_H B^{-1} B \times E_\perp \quad (1)$$

where σ_H and σ_P are the Hall and Pedersen conductivities, respectively, and B is the magnitude of Earth magnetic field. [e.g., *Boström*, 1964; *Burch et al.*, 1976]. Assuming divergence free currents, $\nabla \times j = 0$ or $\nabla \times j_\perp + \nabla \times j_{||} = 0$ (i.e., no accumulation of space charges), and quasi-stationary electric field structures, $\nabla \times \mathrm{E} = \nabla \times \mathrm{E}_\perp + \nabla \times \mathrm{E}_{||}$, we have the following expression for the FAC:

$$-\nabla \cdot j_{||} = \sigma_P \nabla \cdot E_\perp + (\nabla \sigma_P) \cdot E_\perp + (\nabla \sigma_H) B^{-1} (B \times E_\perp) + \sigma_H B^{-1} B \cdot \left(\nabla \times E_{||}\right) \quad (2)$$

Escoubet et al. [1995] found narrow 0.2–1 keV electron precipitation structures on the boundaries of the cusp in 80% of the DE2 cusp/cleft crossings, typically 1 or 2 structures per cusp/cleft crossing, possibly related to shears in plasma convection [*Escoubet et al.*, 1992]. Such low energy electron beams will not give rise to significant enhancements in E-region Hall and Pedersen conductivities. For the events presented here on 16 and 20 December 2001, traces of particle impact ionization were observed down to 140–200 km, i.e., gradients in the electron concentration occurred well above the peak in the Pedersen and Hall mobility coefficients [*Moen and Brekke*, 1990]. Hence the conductivity gradient terms in the second and the third term in equation (2) can be neglected. Furthermore, if we assume no field-aligned acceleration underneath the ESR flow measurements, the fourth term on the right hand side can also be neglected as well and the field-aligned distribution of current density is directly proportional to $\nabla \times E_\perp$ and will hence peak at the flow shear, as actually observed for all the RFE events presented here.

[39] The 10 keV electron beams at night will give rise to strong gradients in the Pedersen conductivity and subsequently a short circuiting effect due to the second term on the right-hand side in equation (2) [*Burch et al.*, 1976]. Auroral potential structures at night are therefore observed as spikes in the E-field [e.g., *Burch et al.*, 1976; *Marklund*, 1984, and references therein]. However, in the cusp ionosphere, an auroral potential structure of a few hundred eV will not give rise to significant modulation in the Pedersen conductivity and is therefore not subject to a significant E-region short cutting effect. A flow shear that develops near a magnetospheric discontinuity will therefore be preserved when mapped down to the ionosphere.

[40] From ground-based data alone we are not in the position to describe the auroral potential region. Features driven by KA waves will generally be highly variable (on second timescales) and have forms/structures generally less than 10 km in width [e.g., *Kletzing*, 1994; *Chaston et al.*, 2007]. The 10–20 min long RFE life time means a quasi-static nature. The half-width of the RFE disturbance is of the order 100–200 km as for inverted Vs [*Lyons*, 1980]. The flow potential across the RFE in Figure 6a is 0.8 kV, i.e., of the same order as the field-aligned potential drop.

[41] All the RFEs covered by optics developed near the OCB, which is an observed feature also for inverted Vs. *Burch et al.* [1990] found that the dayside inverted Vs typically occur on the immediate equatorward side of the cusp/cleft region which contains trapped electrons. *Menietti and Smith* [1993] presented examples of dayside inverted Vs for IMF B_Z negative which they attributed to the low-latitude boundary layer (LLBL), on closed or freshly open flux. As pointed out in a recent work by *Menietti et al.* [2007] it is still not clear if dayside inverted Vs are magnetically connected to reconnection sites or not. *Moen et al.* [2004a] observed the connection between PMAFs and ion up-flow events observed by ESR. The ion up-flow events broadened in a characteristic V-shape consistent with an inverted V-potential structure moving over the radar. However, future work is needed to eventually establish a connection between RFEs and inverted Vs.

5. Summary and Concluding Remarks

[42] Reversed Flow Events (RFEs) are characterized by longitudinally elongated 100–200 km wide channels of 10–20 min life time, i.e., a mesoscale quasi-stationary phenomenon. The direction of zonal motion within the channel opposes the background convection governed by magnetic tension [*Rinne et al.*, 2007]. The RFEs stay in stark contrast to the 3 categories of flow channels reported by *Sandholt et al.* [2004], which all added drive to the large-scale convection. (cf. section 1). In this paper we have performed a detailed examination of this event category by comparing EISCAT Svalbard Radar and all-sky camera observations near winter solstice.

[43] For every RFE there was a thin auroral form aligned with the clockwise convection reversal, consistent with a converging electric field and an upward Birkeland current sheet. The RFE phenomenon appears to be an intimate part of a Birkeland current arc system with a double flow shear, similar to category $\mathrm{II_b}$ in *Marklund* [1984]. As discussed in section 4.2 there are problems with the Southwood FTE interpretation of the RFE phenomenon. The *Southwood* [1987] FTE model is lacking a current sheet to put a latitudinal constraint on the return flow. Instead, the return flows are supposed to broaden very quickly due to incompressibility [*Thorolfsson et al.*, 2000]. In section 4.3 we proposed two alternative explanations for the RFE phenomenon:

[44] (1) The RFE electric field arises in between two large-scale current loops as schematically illustrated in Figure 6c; each mapping to a different boundary layer/reconnection site. Notably the RFE channel is a region void of precipitation and particle impact ionization will not contribute to the Pedersen conductance. This interpretation works only for low Pedersen conductance across RFE channel, which means a summer–winter asymmetry in the occurrence rate.

[45] (2) The quasi-stationary nature and the bipolar form of the RFE flow disturbance seem consistent with an inverted V type potential structure. Inverted Vs is a com-

monly observed phenomenon near the dayside OCB [*Burch et al.*, 1990; *Menietti and Smith*, 1993; *Menietti et al.*, 2007]. Electron beams of <1 keV on the dayside will not give rise to significant conductivity gradients and the shape of the magnetospheric E-field discontinuity will be conserved when mapped down onto the ionosphere. As was noted in Figure 2 the background flow was gradually suppressed (Fs) in the development phase of RFE10. This may indicate a partial decoupling from the magnetosphere due to a field-aligned potential drop.

[46] The two explanations above may be closely related to each other. For example, the discontinuity in the magnetospheric electric field proposed in (1) may be the precondition for the inverted V proposed in (2). Combined ground and in situ observations will be needed to establish the electrodynamic context of the RFE phenomenon, including Alfvén waves and field-aligned acceleration, small and large scale FACs, and how these flow channels map relative to active reconnection sites/FTEs.

[47] We plan to continue SP-FASM experiments at EISCAT Svalbard Radar to search for summer–winter asymmetry in the occurrence rate of reversed flow channels. Although the RFE phenomenon has not yet been reported based on SuperDARN observations, given their spatial dimension and long lifetime they should be observable. For the large scale convection picture the RFEs are negligible. The flow potential of a typical event is ~1 kV. However, this phenomenon may in fact be very important for the production of HF backscatter irregularities in the cusp region. KHI will grow very rapidly at the RFE flow reversals [*Carlson et al.*, 2007].

[48] **Acknowledgments.** EISCAT is an international association supported by research organizations in China (CRIRP), Finland (SA), France (CNRS, till end 2006), Germany (DFG), Japan (NIPR and STEL), Norway (NFR), Sweden (VR), and the United Kingdom (STFC). We thank the ACE Science Center and the ACE MAG and SWEPAM instrument teams for providing data from the ACE space craft. We acknowledge the Johns Hopkins University Applied Physics Laboratory for providing web access to SuperDARN convection maps. Financial support has been provided by the Norwegian Research Council, AFOSR task 2311AS, and Nagoya University.

[49] Wolfgang Baumjohann thanks Eric Lund and Stephan Buchert for their assistance in evaluating this paper.

References

Boström, C. (1964), A model of the auroral electrojets, *J. Geophys. Res.*, *69*, 4983.

Burch, J. L., W. Lennartsson, W. B. Hanson, R. A. Heelis, J. H. Hoffman, and R. A. Hoffman (1976), Properties of Spikeline shear flow reversals observed in the auroral plasma by atmospheric explorer C, *J. Geophys. Res.*, *22*, 3886–3896.

Burch, J. L., J. D. Menietti, and J. A. Slavin (1990), Dayside auroral particle acceleration mechanisms derived from dynamics explorer data, *J. Geomag. Geoelectr.*, *42*, 1365–1378.

Carlson, H. C., K. Oksavik, J. Moen, A. P. van Eyken, and P. Guio (2002), ESR mapping of polar cap patches in the dark cusp, *Geophys. Res. Lett.*, *29*(10), 1386, doi:10.1029/2001GL014087.

Carlson, H. C., T. Pedersen, S. Basu, M. Keskinen, and J. Moen (2007), Case for a new process, not mechanism, for cusp irregularity production, *J. Geophys. Res.*, *112*, A11304, doi:10.1029/2007JA012384.

Chaston, C. C., C. W. Carlson, J. P. McFadden, R. E. Ergun, and R. J. Strangeway (2007), How important are dispersive Alfvèn waves for auroral particle acceleration?, *Geophys. Res. Lett.*, *34*, L07101, doi:10.1029/2006GL029144.

Chiu, M. C., et al. (1998), ACE spacecraft, *Space Sci. Rev.*, *86*, 257–284.

Cowley, S. W. H., J. P. Morelli, and M. Lockwood (1991), Dependence of convective flows and particle precipitation in the high-latitude dayside ionosphere on the X and Y components of the interplanetary magnetic field, *J. Geophys. Res.*, *96*, 5557–5564.

Cowley, S. W. H., and M. Lockwood (1992), Excitation and decay of solar wind-driven flows in the magnetosphere-ionosphere system, *Ann. Geophys.*, *10*, 103–115.

Denig, W. F., W. J. Burke, N. C. Maynard, F. J. Rich, B. Jacobsen, P. E. Sandholt, A. Egeland, S. Leontjev, and V. G. Vorobjev (1993), Ionospheric signatures of dayside magnetopause transients: A case study using satellite and ground measurements, *J. Geophys. Res.*, *98*, 5969–5980.

Doe, R. A., J. D. Kelly, and E. R. Sánchez (2001), Observations of persistent dayside F region electron temperature enhancements associated with soft magnetosheath-like precipitation, *J. Geophys. Res.*, *106*, 3615–3630.

Escoubet, C. P., M. F. Smith, S. F. Fung, P. C. Anderson, R. A. Hoffman, E. M. Basinska, and J. M. Bosqued (1992), Staircase ion signature in the polar cusp: A case study, *Geophys. Res. Lett.*, *19*, 1735–1738.

Escoubet, C. P., M. F. Smith, S. F. Fung, and R. A. Hoffman (1995), Electron structures in the cusp/cleft region observed by DE 2 satellite, *J. Geophys. Res.*, *100*, 1597–1610.

Farrugia, C. J., et al. (2004), Pulsed flows at the high-altitude cusp poleward boundary, and associated ionospheric convection and particle signatures, during Cluster-FAST-SuperDARN-Søndrestrøm conjunction during southwest IMF, *Ann. Geophys.*, *22*, 2891–2905.

Goertz, C. K., E. Nilsen, A. Korth, K. H. Glassmeier, C. Haldoupis, P. Hoeg, and D. Hayward (1985), Observations of possible ground signatures of flux transfer events, *J. Geophys. Res.*, *90*, 4069–4078.

Haerendel, G., G. Pashmann, N. Sckopke, H. Rosenbauer, and P. C. Hedgecock (1978), The frontside boundary layer of the magnetosphere and the problem of reconnection, *J. Geophys. Res.*, *83*, 3195–3216.

Kletzing, C. A. (1994), Electron acceleration by kinetic Alfvèn waves, *J. Geophys. Res.*, *99*, 11,095–11,103.

Lin, C. S., and R. A. Hoffman (1982), Observations of inverted-V electron precipitation, *Space Sci. Rev.*, *33*, 415–457.

Lockwood, M., and M. F. Smith (1992), The variation of reconnection rate at the dayside magnetopause and cusp ion precipitation, *J. Geophys. Res.*, *97*, 14,841–14,847.

Lockwood, M., P. E. Sandholt, S. W. H. Cowley, and T. Oguti (1989), Interplanetary magnetic field control of dayside auroral activity and the transfer of momentum across the dayside magnetopause, *Planet. Space Sci.*, *37*, 1347–1365.

Lockwood, M., S. W. H. Cowley, P. E. Sandholt, and R. P. Lepping (1990), The ionospheric signatures of flux transfer events and solar wind dynamic pressure changes, *J. Geophys. Res.*, *95*, 17,113–17,135.

Lockwood, M., J. Moen, S. W. H. Cowley, A. D. Farmer, U. P. Løvhaug, H. Lühr, and V. N. Davda (1993), Variability of dayside convection and motions of the cusp/cleft aurora, *Geophys. Res. Lett.*, *20*, 1011–1014.

Lockwood, M., S. E. Milan, T. Onsager, C. H. Perry, J. A. Scudder, C. T. Russell, and M. Brittnacher (2001), Cusp ion steps, field aligned currents and poleward moving auroral forms, *J. Geophys. Res.*, *106*, 29,555–29,569.

Lyons, L. (1980), Generation of large-scale regions of auroral currents, electric potentials, and precipitation by the divergence of the convection electric field, *J. Geophys. Res.*, *85*, 17–24.

Marklund, G. (1984), Auroral arc classification scheme on the observed arc-associated electric field pattern, *Planet. Space Sci.*, *32*, 193–211.

Marchaudon, A., J.-C. Cerisier, R. A. Greenwald, and G. J. Sofko (2004), Electrodynamics of a flux transfer event; Experimental test of the Southwood model, *Geophys. Res. Lett.*, *31*, L09809, doi:10.1029/2004GL019922.

McComas, D. J., S. J. Bame, P. Barker, W. C. Feldman, J. L. Phillips, P. Riley, and J. W. Griffee (1998), Solar wind electron proton alpha monitor (SWEPAM) for the advanced composition explorer, *Space Sci. Rev.*, *86*, 563–612.

McWilliams, K. A., T. K. Yoeman, and S. W. H. Cowley (2001), Two-dimensional electric field measurements in the ionospheric footprint of a flux transfer event, *Ann. Geophys.*, *19*, 1584–1598.

Menietti, J. D., and M. F. Smith (1993), Inverted Vs spanning the cusp boundary layer, *J. Geophys. Res.*, *98*, 11,391–11,400.

Menietti, J. D., R. A. Frahm, A. Korth, F. S. Mozer, and Y. Khotyaintsev (2007), Polar and cluster observations of a dayside inverted-V during conjunction, *Ann. Geophys.*, *25*, 543–555.

Milan, S. E., M. Lester, S. W. H. Cowley, J. Moen, P. E. Sandholt, and C. J. Owen (1999), Meridian-scanning photometer, coherent HF radar, and magnetometer observations of the cusp: A case study, *Ann. Geophys.*, *17*, 159–172.

Milan, S. E., M. Lester, S. W. H. Cowley, and M. Brittnacher (2000), Convection and auroral response to a southward turning of the IMF: Polar UVI, CUTLASS, and IMAGE signatures of transient magnetic flux transfer at the magnetopause, *J. Geophys. Res.*, *105*, 15,741–15,755.

Moen, J., and A. Brekke (1990), On the importance of ion composition to conductivities in the auroral ionosphere, *J. Geophys. Res.*, *95*, 10,687–10,693.

Moen, J., P. E. Sandholt, M. Lockwood, W. F. Denig, U. P. Løvhaug, B. Lybekk, A. Egeland, D. Opsvik, and E. Friis-Christensen (1995), Events of enhanced convection and related dayside auroral activity, *J. Geophys. Res.*, *100*, 23,917–23,934.

Moen, J., D. Evans, H. C. Carlson, and M. Lockwood (1996), Dayside moving auroral transients related to LLBL dynamics, *Geophys. Res. Lett.*, *23*, 3247–3250.

Moen, J., D. A. Lorentzen, and F. Sigernes (1998), Dayside moving auroral forms and bursty proton auroral events in relation to particle boundaries observed by NOAA-12, *J. Geophys. Res.*, *103*, 14,855–14,863.

Moen, J., A. P. van Eyken, and H. C. Carlson (2001), EISCAT Svalbard Radar observations of ionospheric plasma dynamics in relation to dayside auroral transients, *J. Geophys. Res.*, *106*, 21,453–21,461.

Moen, J., K. Oksavik, and H. C. Carlson (2004a), On the relationship between ion upflow events and cusp auroral transients, *Geophys. Res. Lett.*, *31*, L11808, doi:10.1029/2004GL020129.

Moen, J., M. Lockwood, K. Oksavik, H. C. Carlson, W. F. Denig, A. P. van Eyken, and I. W. McCrea (2004b), The dynamics and relationships of precipitation, temperature and convection boundaries in the dayside auroral ionosphere, *Ann. Geophys.*, *22*, 1973–1987.

Moen, J., H. C. Carlson, K. Oksavik, C. P. Nielsen, S. E. Pryse, H. R. Middleton, I. W. McCrea, and P. Gallop (2006), EISCAT observations of plasma patches at sub-auroral cusp latitudes, *Ann. Geophys.*, *24*, 2363–2374.

Neudegg, D. A., et al. (2000), A survey of magnetospause FTEs and associated flow bursts in the polar ionosphere, *Ann. Geophys.*, *18*, 416–435.

Nilsson, H., M. Yamauchi, L. Eliasson, O. Norberg, and J. Clemmons (1996), Ionospheric signature of the cusp as seen by incoherent scatter radar, *J. Geophys. Res.*, *101*, 10,947–10,963.

Oksavik, K., J. Moen, and H. C. Carlson (2004), High-resolution observations of the small-scale flow pattern associated with a poleward moving auroral form in the cusp, *Geophys. Res. Lett.*, *31*(11), L11807, doi:10.1029/2004GL019838.

Oksavik, K., J. Moen, H. C. Carlson, R. A. Greenwald, S. E. Milan, M. Lester, W. F. Denig, and R. J. Barnes (2005), Multi-instrument mapping of the small-scale flow dynamics related to a cusp auroral transient, *Ann. Geophys.*, *23*, 2657–2670.

Pinnock, M., A. S. Rodger, J. R. Dudeney, K. B. Baker, P. T. Newell, R. A. Greenwald, and M. E. Greenspan (1993), Observations of an enhanced convection channel in the cusp ionosphere, *J. Geophys. Res.*, *98*, 3767–3776.

Pinnock, M., A. S. Rodger, J. R. Dudeney, F. Rich, and K. B. Baker (1995), High spatial and temporal resolution of the ionospheric cusp, *Ann. Geophys.*, *13*, 919–925.

Provan, G., and T. K. Yoeman (1999), Statistical observations of the MLT, latitude and size of pulsed ionospheric flows with the CUTLASS Finland radar, *Ann. Geophys.*, *17*, 855–867.

Provan, G., T. K. Yoeman, and S. E. Milan (1998), CUTLASS Finland radar observations of the ionospheric signatures of flux transfer events and the resulting plasma flows, *Ann. Geophys.*, *16*, 1411–1422.

Pryse, S. E., A. M. Smith, L. Kersley, I. K. Walker, C. N. Mitchell, J. Moen, and R. W. Smith (2000), Multi-instrument probing of the polar ionosphere under steady northward IMF, *Ann. Geophys.*, *18*, 90–98.

Rinne, Y., J. Moen, K. Oksavik, and H. C. Carlson (2007), On the occurrence of reversed flow events in the cusp ionosphere observed by european incoherent scatter (EISCAT) Svalbard radar, *J. Geophys. Res.*, *112*, A10313, doi:10.1029/2007JA012366.

Ruohoniemi, J. M., and K. B. Baker (1998), Large-scale imaging of high-latitude convection with super dual auroral radar network HF radar observations, *J. Geophys. Res.*, *103*, 20,797–20,811.

Russell, C. T., and R. C. Elphic (1979), ISEE observations of flux transfer events at the dayside magnetopause, *Geophys. Res. Lett.*, *6*, 33–36.

Sandholt, P. E., and C. J. Farrugia (2007), Role of poleward moving auroral forms in the dawn-dusk auroral precipitation asymmetries induced by IMF B_Y, *J. Geophys. Res.*, *112*, A04203, doi:10.1029/2006JA011952.

Sandholt, P. E., M. Lockwood, T. Oguti, S. W. H. Cowley, K. S. C. Freeman, B. Lybekk, A. Egeland, and D. M. Willis (1990), Midday auroral breakup events and related energy and momentum transfer from the magnetosheath, *J. Geophys. Res.*, *95*, 1039–1060.

Sandholt, P. E., J. Moen, A. Rudland, D. Opsvik, W. F. Denig, and T. Hansen (1993), Auroral event sequences at the dayside polar cap boundary for positive and negative IMF B_Y, *J. Geophys. Res.*, *98*, 7737–7755.

Sandholt, P. E., C. J. Farrugia, J. Moen, Ø. Noraberg, B. Lybekk, T. Sten, and T. L. Hansen (1998), A classification of dayside auroral forms and activities as a function of IMF orientation, *J. Geophys. Res.*, *103*, 23,325–23,345.

Sandholt, P. E., C. J. Farrugia, and W. F. Denig (2004), Detailed dayside auroral morphology as a function of local time for southeast IMF orientation: Implications for solar wind coupling, *Ann. Geophys.*, *22*, 3537–3560.

Smith, C. W., J. L'Heureux, N. F. Ness, M. H. Acuna, L. F. Burlaga, and J. Scheifele (1998), The ACE magnetic fields experiment, *Space Sci. Rev.*, *86*, 613–632.

Southwood, D. J. (1987), The ionospheric signature of flux transfer events, *J. Geophys. Res.*, *92*, 3207–3213.

Stern, D. (1984), Magnetospheric dynamo processes, in *Magnetospheric Currents*, *Geophys. Monogr. Ser.*, vol. 28, edited by T. Potemra, pp. 200–207, AGU, Washington, D. C.

Taguchi, S., M. Sugiura, J. Winningham, and J. Slavin (1993), Characterization of the IMF B_Y-dependent filed-aligned currents in the cleft region based on DE 2 observations, *J. Geophys. Res.*, *98*, 1393–1407.

Thorolfsson, A., J.-C. Cerisier, M. Lockwood, P. E. Sandholt, C. Senior, and M. Lester (2000), Simultaneous optical and radar signatures of poleward moving auroral forms, *Ann. Geophys.*, *18*, 1054–1066.

Waterman, J., D. Lummerzheim, O. de la Beaujardiere, P. T. Newell, and F. J. Rich (1994), Ionospheric footprint of magnetosheathlike particle precipitation observed by an incoherent scatter radar, *J. Geophys. Res.*, *99*, 3855–3867.

H. C. Carlson, J. Moen, and Y. Rinne, Department of Physics, University of Oslo, Sem Saelandsvei 24, P.O. Box 1048, Blindern, N-0316, Oslo Norway. (jmoen@fys.uio.no)

R. Fujii, Solar-Terrestrial Environmental Laboratory, Nagoya University, Chikusa-ku, Nagoya 464-8602, Japan.

K. Oksavik, Arctic Geophysics, The University Centre in Svalbard, P.O. Box 156, Longyearbyen, N-9171 Svalbard, Norway.

H. Opgenoorth, European Space Agency, ESTEC (SCI/SM), P.O. Box 299, 2200 AG Noordwijk, Netherlands.